Initial- and final-state alignment and orientation effects in Ca energy pooling

Harold V. Parks and Stephen R. Leone
JILA, University of Colorado and National Institute of Standards and Technology and Department of Physics, University of Colorado, Boulder, Colorado 80309-0440
(Received 12 April 1999)

An experimental investigation is performed to determine the initial- and final-state alignment effects in the energy-pooling process $Ca(4s4p\ ^3P_1)+Ca(4s4p\ ^3P_1)\rightarrow Ca(4s4p\ ^1P_1)+Ca(4s^2)$. This paper represents a type of four-vector correlation experiment, where two aligned atoms collide and the alignment of the final excited state is observed. The initial $Ca(4s4p\ ^3P_1)$ state polarization is controlled with polarized lasers and magnetic fields, and the final-state alignment is partially resolved by observing the polarization of the fluorescence from the $Ca(4s4p\ ^1P_1)\rightarrow Ca(4s^2)$ emission. The mathematics are developed in this paper to provide a full quantitative description of the four-vector alignment cross sections observed here. Relative values that describe 18 of the 39 total independent parameters are obtained, thus defining the results of this collision process at an unprecedented level of detail. The final-state Ca polarization is found to be only weakly dependent on the initial-state alignment, with final-state fluorescence predominately polarized along the relative velocity vector of the collision. [S1050-2947(99)00510-7]

PACS number(s): 34.50.Pi, 34.50.Rk

I. INTRODUCTION

Laser-alignment experiments provide a powerful method to study atomic interactions and the dynamics of collision processes [1–4]. In these experiments, the colliding atoms are prepared in an electronic state with well-defined energy and angular momentum before the collision. This influences the molecular states that are explored during the collision. By changing the laser polarization, different angular momentum states can be created. Thus, there is partial control over the molecular states involved when two atoms collide. The most common type of vector-correlation experiment involves control of only two vectors, the initial relative velocity of the colliding atoms and the alignment of one of the atoms before the collision [5–7]. Less frequent are three-vector experiments. Experiments performed on the extensively studied $Na(3p)+Na(3p)$ associative ionization system [8–10] represent one type of a three-vector experiment, where the initial alignment of both the colliding atoms together with the initial relative velocity are controlled. This type of three-vector experiment was also performed for the energy-pooling process:

$$Ca(4s4p\ ^3P_1)+Ca(4s4p\ ^3P_1)\rightarrow Ca(4s4p\ ^1P_1)+Ca(4s^2\ ^1S_0), \quad (1)$$

in previous work by this group [11]. This paper will be subsequently referred to as Parks *et al.* There are only a few examples of four-vector experiments in the literature. These involve the initial and final velocity together with initial and final alignments [12–14]. In this paper we perform a type of four-vector experiment by extending the experiments of Parks *et al.* Not only is the alignment of both initial states with respect to the relative velocity vector of the collision controlled, but now the alignment of the final $Ca(4s4p\ ^1P_1)$ state is also partially resolved. In addition, the mathematics are developed in this paper to quantify the detailed results obtained here and to relate them to the individual cross-section parameters for four-vector correlations.

As in Parks *et al.*, the initial-state alignment is controlled with a polarized laser and weak-magnetic fields. The $Ca(4s4p\ ^3P_1)$ states are excited with a pulsed dye laser. The polarization of this laser beam creates states with a specific alignment. After the laser pulse, the atoms precess in a weak-magnetic field, allowing different alignments to be sampled at different time delays after the laser pulse. The relative energy-pooling rates are determined by observing fluorescence on the $Ca(4s4p\ ^1P_1)\rightarrow Ca(4s^2\ ^1S_0)$ transition. In order to detect the final-state alignment, a polarizer is placed between the photodetector and the collision region. In this experiment, all of the initial states are prepared in the same alignment by the laser. However, a technique involving a magnetic-field gradient allows atoms with different alignments also to collide at various times after the laser pulse. In order to describe quantitatively the experimental results obtained here, which contain information about a very large number of cross sections, a mathematical framework is developed. The methods of Driessen and co-workers [15,16] are extended to cover the four-vector experiment described here.

Section II of this paper describes the experimental apparatus. The concept of the fundamental cross section is introduced in Sec. III to describe quantitatively the four-vector alignment effects of this experiment. These cross sections are used to reanalyze some of the data from Parks *et al.*, where the issue of possible azimuthal alignment is addressed. Also, this mathematical framework is used to derive the form of the signal for the experiments where the final-state alignment is detected. In Sec. IV the results of the experiments are reported. Next, the use of a magnetic-field gradient is described in Sec. V. Finally in Sec. VI the results are summarized in terms of the fundamental cross sections, and concluding remarks are made in Sec. VII. Appendices A and B report the derivation of the fundamental cross sections in terms of the transition-matrix elements and the results of

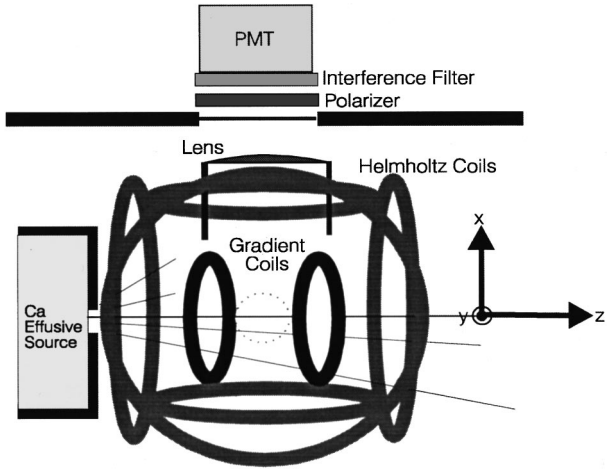

FIG. 1. A schematic diagram of the apparatus. The Ca beam emerges from a small hole in an oven. A 10-cm focal-length lens focuses the Ca fluorescence onto the PMT, and an interference filter is placed in front the PMT to select the 423-nm fluorescence from the final state. Three orthogonal Helmholtz coils are placed around the interaction region to control the magnetic field. In the descriptions used in this paper, the *z* axis is defined to lie in the direction of the Ca beam propagation, the *x* axis points from the collision region to the lens, and the *y* axis is parallel to the laser-beam propagation (pointing out of the page).

how the fundamental cross sections are related to the measured experimental parameters, respectively. The latter expression is used in Sec. III.

II. EXPERIMENTAL APPARATUS

The apparatus has been described in detail in Parks *et al.* and is only outlined here. A schematic is shown in Fig. 1. Energy-pooling collisions are studied in a single atomic beam following pulsed laser excitation. The Ca beam is produced by an oven heated to 975 K. The Ca atoms emerge from a 1-mm×2-mm nozzle that is heated to a slightly higher temperature, 1020 K, to prevent clogging. Under these conditions, the density in the collision region is approximately 8×10^{10} Ca atoms/cm^3, low enough for single-collision conditions to prevail during the time scale of the experiment. Also, the atomic beam defines the *z* axis for this experiment; the relative velocity vector of the collisions must lie along this axis.

Initial states are prepared by pumping $\mathrm{Ca}(4s^2\ ^1S_0) \rightarrow \mathrm{Ca}(4s4p\ ^3P_1)$ with a 5-ns pulse from a dye laser tuned to 657 nm. This laser is either circularly or linearly polarized, resulting in a population of initial states all with the same alignment. After the laser pulse, the $\mathrm{Ca}(4s4p\ ^3P_1)$ initial states precess (with a period of about 0.8 μs) in a magnetic field imposed by a set of Helmholtz coils. This precession allows different alignments to be compared in a single laser pulse. The lifetime of the initial state is 2 ms, but the atoms only remain in the observation region for about 10 μs. The final $\mathrm{Ca}(4s4p\ ^1P_1)$ state, which is populated by energy pooling, decays in a very short time, 4 ns.

In addition to the Helmholtz coils, a set of small coils are used to produce a magnetic-field gradient. The diameter of these coils is 5.5 cm, the separation, from coil center to coil center is 2.45 cm, and the thickness of the coils in the *z* direction is 1 cm. The upstream coil has 100 windings and the downstream coil has 29 windings. These coils produce a magnetic gradient directed along the collision axis, with the derivative of the field constant to within 15% in the collision region. A current of either 0.15 A or 0.30 A is passed through these two coils to produce magnetic fields with an average strength of 3.5 G or 7 G and gradients of 0.75 G/cm or 1.5 G/cm, respectively. The condenser lens used in Parks *et al.* would distort the polarization of the collected fluorescence, so it is replaced by a 10-cm focal-length lens. A polarizer is placed between the collision region and the photomultiplier tube (PMT). A stepper motor allows the polarizer to be rotated. An interference filter is placed in front of the PMT to pass only the final-state fluorescence.

III. FOUR-VECTOR CORRELATION THEORY

A. Fundamental cross sections

A framework is introduced for quantitatively describing the alignment and orientation effects when both $4s4p\ ^3P_1$ initial states are polarized and the final-state alignment of the $4s4p\ ^1P_1$ state is observed. This discussion is based upon the work of Driessen and co-workers [15,16], who applied the analysis of Alexander, Dagdigian, and DePristo [17] and others [18,19]. Originally, this is based upon the methods introduced by Arthurs and Dalgarno [20]. If the energy-pooling cross section is averaged over all final-state alignments the results of Nienhuis can be recovered [21], although that analysis used slightly different methods.

The alignment effects can be described by a set of fundamental cross sections. In terms of these fundamental cross sections, σ, the experimentally observed cross section can be written

$$\sigma_{\mathrm{exp}}=\sum_{m_1,m_1',m_2,m_2'}\rho_{m_1m_1'}\rho_{m_2m_2'}\rho_{m_3m_3'}\sigma_{m_1m_2m_3;m_1'm_2'm_3'}. \qquad (2)$$

Here, m_1, m_2, and m_3 are the m_j magnetic quantum numbers of the initial states of the two colliding atoms and the final state of the $4s4p\ ^1P_1$ atom, respectively. The quantization axis lies along the relative velocity vector of the collision; in this case the collision frame is the axis of the single effusive beam. Also $\rho_{m_1m_1'}$, $\rho_{m_2m_2'}$, and $\rho_{m_3m_3'}$, are the density matrices that describe the two initial and one final electronic angular momentum states of the atoms.

As shown in Appendix A, the fundamental cross sections, $\sigma_{m_1m_2m_3;m_1'm_2'm_3'}$, are given by

$$\begin{aligned}\sigma_{m_1m_2m_3;m_1'm_2'm_3'} &= \frac{1}{k_i^2}\sum_{\substack{j,j',j'',j''',\\ m_l',J,J',\\ l,l',l'',M,M'}} i^{l-l''}(-1)^{j+j''+j'+j'''-m-m'} \\ &\times\pi\sqrt{2l+1}\sqrt{2l''+1}(2J+1)(2J'+1) \\ &\times\begin{pmatrix} j & l & J \\ m_1+m_2 & 0 & -M\end{pmatrix}\begin{pmatrix} 1 & l' & J \\ m_3 & m_l' & -M\end{pmatrix}\end{aligned}$$

$$\times\begin{pmatrix} 1 & 1 & j \\ m_1 & m_2 & -M \end{pmatrix}\begin{pmatrix} j'' & l'' & J' \\ m_1'+m_2' & 0 & -M' \end{pmatrix}$$
$$\times\begin{pmatrix} 1 & l' & J' \\ m_3' & m_1' & -M' \end{pmatrix}\begin{pmatrix} 1 & 1 & j'' \\ m_1' & m_2' & -M' \end{pmatrix}$$
$$\times T^J_{jl;l'} T^{J*}_{j''l'';l'}, \tag{3}$$

where $T^J_{jl;l'}$ is the transition matrix, and the initial-state wave vector is k_i. The other symbols used in Eq. (3) are as follows: j and j' are the total electronic angular momenta of the colliding system for the m_1+m_2 and $m_1'+m_2'$ states, respectively. Also, l and l' are the total orbital angular momenta (of the two atoms) for the m_1+m_2 and $m_1'+m_2'$ states, respectively. J, J', M, and M' are the corresponding total (electronic plus orbital) angular momenta of the colliding system. The initially prepared state may be a superposition of different m_1+m_2 states. Likewise, the final state that is detected may be a superposition of different m_3 states. Thus the unprimed and singly primed quantities represent two interfering pathways from the initial state to the final detected state if $(m_1,m_2,m_3)\neq(m_1',m_2',m_3')$. Finally, j'' and l'' are the electronic and orbital momenta of the excited atom after the collision.

There are a large number of fundamental cross sections, 3^6, but the number of nonzero independent cross sections is considerably less. A fundamental property of the $3j$ symbols is that the bottom row must add to zero. From the first $3j$ symbol this gives $M=m_1+m_2$, and from the fourth $3j$ symbol, $M'=m_1'+m_2'$. Then, from the second and fifth $3j$ symbols, we get

$$\sigma_{m_1m_2m_3;m_1'm_2'm_3'}=0$$

unless

$$m_1+m_2-m_3=m_1'+m_2'-m_3'. \tag{4}$$

Also, it can easily be shown that

$$\sigma_{m_1m_2m_3;m_1'm_2'm_3'}=\sigma_{m_1'm_2'm_3';m_1m_2m_3}^{*}, \tag{5}$$

$$\sigma_{m_1m_2m_3;m_1'm_2'm_3'}=\sigma_{-m_1-m_2-m_3;-m_1'-m_2'-m_3'}, \tag{6}$$

and

$$\sigma_{m_1m_2m_3;m_1'm_2'm_3'}=\sigma_{m_2m_1m_3;m_2'm_1'm_3'}. \tag{7}$$

Finally, there is one additional relation between the cross sections. We follow Driessen and Eno [15], who proved a similar relation for the case where there is only one initially aligned state. Consider the scattering amplitude, $f_{m_1m_2\lambda_f m}(\theta,\varphi)$, given by Eq. (A2) of Appendix A, for the particular case that $m_1+m_2=m_3$. This is

$$f_{m_1m_2\lambda_f m}(\theta,\varphi)=\frac{1}{\sqrt{k_ik_f}}\sum_{\substack{j,j',J,\\ l,l',M}} i^{l-l'+1}(-1)^{j+j'+j_1-j_2-m}$$
$$\times\sqrt{\pi}\sqrt{2l+1}(2J+1)T^J_{jl\lambda_i;1l'\lambda_f}Y_{l'0}(\theta,\varphi)$$
$$\times\begin{pmatrix} j & l & J \\ m & 0 & -m \end{pmatrix}\begin{pmatrix} 1 & l' & J \\ m & 0 & -m \end{pmatrix}$$
$$\times\begin{pmatrix} 1 & 1 & j \\ m_1 & m_2 & -m \end{pmatrix}, \tag{8}$$

where $m=m_1+m_2$. If we take $m_1\rightarrow -m_1$, $m_2\rightarrow -m_2$, and $m_2\rightarrow -m_3$, then using the general property of the $3j$ symbols that

$$\begin{pmatrix} j_1 & j_2 & j_3 \\ -m_1 & -m_2 & -m_3 \end{pmatrix}=(-1)^{j_1+j_2+j_3}\begin{pmatrix} j_1 & j_2 & j_3 \\ m_1 & m_2 & m_3 \end{pmatrix}, \tag{9}$$

the scattering amplitude goes to

$$f_{-m_1-m_2\lambda_f-m}(\theta,\varphi)\rightarrow(-1)^{l+l'+1}f_{m_1m_2\lambda_f m}(\theta,\varphi). \tag{10}$$

Now, the parity of the initial-state electronic wave function is even, and the parity of the final electronic state is odd. This means that in order to conserve total parity, $l+l'$ must be odd. This gives one final relation between the cross sections:

$$\sigma_{-m_1-m_2-m_3;m_1'm_2'm_3}=\sigma_{m_1m_2m_3;m_1'm_2'm_3} \quad \text{if } m_1+m_2=m_3. \tag{11}$$

Using Eqs. (4)–(7) and Eq. (11), there are 39 parameters needed to describe this four-vector collision process. These are represented by 15 real-valued fundamental cross sections:

$$\sigma_{000},\ \sigma_{001},\ \sigma_{010},\ \sigma_{011},\ \sigma_{01-1},\ \sigma_{110},\ \sigma_{111},$$
$$\sigma_{11-1},\ \sigma_{1-10},\ \sigma_{1-11},\ \sigma_{1-10;-110},\ \sigma_{1-11;-111},$$
$$\sigma_{010;100},\ \sigma_{011;101},\ \text{and}\ \sigma_{01-1;10-1}, \tag{12}$$

and 12 complex valued cross sections:

$$\sigma_{000;1-10},\ \sigma_{001;1-11},\ \sigma_{110;01-1},\ \sigma_{111;010},\ \sigma_{1-11;0-10},$$
$$\sigma_{1-11;010},\ \sigma_{1-10;011},\ \sigma_{100;00-1},\ \sigma_{000;011},\ \sigma_{111;00-1},$$
$$\sigma_{1-11;001},\ \text{and}\ \sigma_{1-1-1;111}. \tag{13}$$

In the notation used here $\sigma_{m_1m_2m_3}=\sigma_{m_1m_2m_3;m_1m_2m_3}$, which is called a conventional cross section. It represents the energy-pooling cross section for an atom in the state m_1 colliding with an atom in the state m_2. The cross section $\sigma_{m_1m_2m_3;m_1'm_2'm_3'}$, when $(m_1,m_2,m_3)\neq(m_1',m_2',m_3')$, is called a coherence cross section and represents the contribution from the interference between an $m_1+m_2\rightarrow m_3$ collision and an $m_1'+m_2'\rightarrow m_3'$ collision.

B. A reanalysis of previous data

A type of four-vector experiment was already described in Parks *et al.* In that experiment two aligned atoms are collided and the azimuthal variation in the final-state fluorescence was investigated. This experiment is reanalyzed in terms of the fundamental cross sections of Sec. III A and it is demonstrated here that there is a slight final-state alignment effect. In the next section, experiments are described that provide much more information on the final-state alignment.

Consider first the reanalysis of Parks *et al.* If Ca atoms are excited from the ground s state to a p state with a linearly polarized laser, a pure $m_j=0$ excited state is produced when the polarization is parallel to the quantization axis. The symmetry axis of the orbital is defined to be the quantization axis that, at any instant, gives a pure $m_j=0$ state. In the experiment, the initial-state atoms are excited so that their symmetry axis lies in the x-y plane (perpendicular to the z axis). With linear excitation polarization, this is accomplished by polarizing the laser beam along the x axis. With circular polarization, the laser beam is polarized around the y axis. In this case, the symmetry axis is defined to be the axis around which the atoms are in a pure $m_j=1$ state. For both the linear and circular cases, a magnetic field is directed along the z axis causing the symmetry axis to precess in the x-y plane (always remaining perpendicular to the z axis).

The fluorescence from the final $4s4p\ ^1P_1$ state is observed with a detector that lies in the x direction from the collision region. Fluorescence from the p_y and p_z states is observed with equal probability, but no fluorescence is detected from the p_x state. Note also that the alignment of the initial states is the only thing that breaks the azimuthal symmetry of the colliding system. This means that the precession of the electronic states can be thought of as equivalent to rotating the detector around the collision region while the symmetry axis is held fixed. In this way, azimuthal variations in the final-state fluorescence can be mapped out. Inserting the appropriate density matrices into Eq. (2), we find the signal (proportional to the cross sections) as a function of time will be

$$I(t)=m_{l,c}+n_{l,c}\cos 2\omega t, \tag{14}$$

where ω is the precession frequency in the magnetic field,

$$\omega=\mu_B g B/\hbar. \tag{15}$$

Here μ_B is the Bohr magneton and g is the Lande factor. In the case of linearly polarized excitation, the relationship between the measured parameters and the desired cross sections is rather limited because of the complexity:

$$m_l=\tfrac{1}{8}\sigma_{111}+\tfrac{1}{4}\sigma_{1-10}+\tfrac{1}{4}\sigma_{1-11}+\tfrac{1}{4}\sigma_{110}+\tfrac{1}{8}\sigma_{111}+\tfrac{1}{4}\sigma_{1-11;-111}+\tfrac{1}{4}\sigma_{1-10;-110},$$

$$n_l=-\tfrac{1}{2}\sigma_{111;1-1-1}. \tag{16}$$

In the case of circular polarization, the parameters m_c and n_c are again linear combinations of the cross sections in Eqs. (12) and (13). The equations for these parameters are more complicated than Eq. (16), and are given in Appendix B.

The results of the experiment are shown in Fig. 2. There is no detectable modulation seen in the linear case. This means that the value of n_l is too small to be detected. In this experiment, we are only looking for relative modulations, since we do not measure the absolute size of the signal. That is, we have not determined n_l, but rather n_l/m_l. The measured value for this parameter is $n_l/m_l=0.000\pm0.008$. The uncertainty here is derived from the error in the direction of the magnetic field. The uncertainty in the magnetic-field alignment is $\pm10°$. If the field is not directed exactly along the z axis, the symmetry axis will wobble slightly in and out of the x-y plane. From the data obtained in Parks *et al.* it was found that any time the angle between the symmetry axis and the z axis changes, there is a modulation in the energy-pooling signal. In this case, a 10° misalignment of the magnetic field would result in a 0.008 relative modulation in the energy-pooling signal. This then represents the lowest limit on the real modulation signal that can be detected reliably.

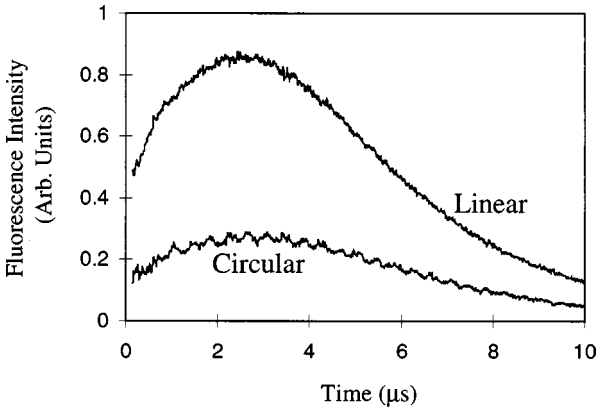

FIG. 2. The data from Parks *et al.* where no final-state polarizer is used and the magnetic field is directed along the z axis [11]. This tests for azimuthal alignment in the final state. No modulation is seen in the linear case, but a small amount of modulation is seen in the circular case.

In the circular case, small but distinct modulations can be seen in Fig. 2. The amplitude of these oscillations is $n_c/m_c=-0.04\pm0.02$. The negative sign means that the signal is at a minimum when the symmetry axis is pointing at the detector (along the x axis) and maximum when the symmetry axis is parallel with the y axis. The uncertainty quoted here is again the modulation that would result from a 10° misalignment in the magnetic field. This uncertainty is larger than in the linear case, because, as seen in Parks *et al.*, the circular signal is much more strongly dependent on the angle between the symmetry axis and the z axis. A careful analysis of the circular data also reveals a modulation with a period equal to one full precession around the z axis, as opposed to twice this period as expected by Eq. (14). However, it can be shown that this spurious modulation can be explained by a magnetic-field misalignment, which is well within the $\pm10°$ error range.

While the connection to the fundamental cross sections is complex, the results do show that there is a four-vector correlation effect. This section serves as a first example of the four-vector correlation theory developed in the last section. Even though no large final-state alignment is observed here, this experiment represents one small piece of the larger pic-

ture that will be expanded upon in the next experiments. The fit parameters found in this section will be used together with the results of the next experiments to solve for the values of the fundamental cross sections, as given in the conclusion. We do already have the value of one fundamental cross section. Since n_l/m_l is very small, it is immediately seen from Eq. (16) that $\sigma_{111;1-1-1}$ must also be very small.

C. Polarized final-state detection

We now turn to a type of experiment that permits the extraction of much more cross-section information. Here the initial-state atoms are excited with a laser linearly polarized along the z axis (parallel to the relative velocity vector), and a magnetic field is directed along the x axis. Thus, the symmetry axis of the electronic state remains in the y-z plane and precesses around the x axis. The final-state fluorescence detector is located along the x axis from the collision region. A polarizer is placed between the detector and the collision region with its axis making an angle θ with the x-z plane. In the case of linearly polarized excitation, Eq. (2) gives a signal:

$$I(t)=(d_l+e_l\cos 2\theta)\cos 2\omega t+f_l\sin 2\theta\sin 2\omega t + (g_l+h_l\cos 2\theta)\cos 4\omega t+j_l\sin 2\theta\sin 4\omega t+k_l + l_l\cos 2\theta. \quad (17)$$

The parameters $d_l,\ldots,l_l$ are equal to linear combinations of the fundamental cross sections listed in Eqs. (12) and (13). These relationships are quite complicated and are given in Appendix B. Here, ωt is the angle between the z axis and the symmetry vector, if the laser pulse is at $t=0$. The precession frequency is again given by Eq. (15). When the linearly polarized laser beam is replaced with a laser beam that is circularly polarized around the y axis, we get an expression with the same form but different coefficients, (Appendix B):

$$I(t)=(d_c+e_c\cos 2\theta)\cos 2\omega t+f_c\sin 2\theta\sin 2\omega t + (g_c+h_c\cos 2\theta)\cos 4\omega t+j_c\sin 2\theta\sin 4\omega t + k_c+l_c\cos 2\theta. \quad (18)$$

Strictly speaking, if $t=0$ is to be defined as the time when the laser pulse occurs, ωt in Eq. (18) should be replaced by $\omega t+\pi/2$, because the laser is circularly polarized around the y axis. Thus, at $t=0$ the symmetry vector is perpendicular to the z axis. However, in practice the time origin is defined by fitting the signal, averaged over θ, to Eq. (18). Also it can be seen from the equations in Appendix B that

$$g_l=4g_c,\quad h_l=4h_c,\quad \text{and } j_l=4j_c. \quad (19)$$

A number of parameters can now be obtained by fitting the observed data to the forms in Eqs. (17) and (18) and the physical meaning of these parameters is examined briefly.

D. The meaning of the alignment parameters

There are the two parameters $n_{l,c}$ and $m_{l,c}$ that describe the modulation in the signal when the system is rotated around the z axis. These were described in the last subsection. Then we obtain the parameters $d_{l,c}$, $g_{l,c}$, and $k_{l,c}$. If we average Eqs. (17) and (18) over θ, then all the terms that depend on θ average to zero and we get

$$I(t)=d_{l,c}\cos(2\omega t)+g_{l,c}\cos(4\omega t)+k_{l,c}. \quad (20)$$

This is exactly the form for the signal observed in Parks *et al.* when the polarization of the final-state fluorescence is not resolved. This is not surprising since without the detector polarizer the observed fluorescence is averaged over all θ. Thus the parameters $d_{l,c}$, $g_{l,c}$, and $k_{l,c}$ have already been obtained in the data of Parks *et al.* In addition, if Eqs. (17) and (18) are averaged over all ωt we can extract $k_{l,c}+l_{l,c}\cos(2\theta)$. Thus, the parameter $l_{l,c}$ describes how the mean signal, averaged over the modulations due to the magnetic precession, varies as the detector polarizer is rotated. Finally the parameters $e_{l,c}$, $h_{l,c}$, $f_{l,c}$, and $j_{l,c}$ describe how the modulations due to the magnetic precession change as the detector polarizer is rotated. The parameters $e_{l,c}$, and $h_{l,c}$ describe the modulation of the $\cos 2\omega t$ and $\cos 4\omega t$ terms, respectively. Also, $f_{l,c}$, and $j_{l,c}$ give the modulation of the $\sin 2\omega t$ and $\sin 4\omega t$ terms, respectively. Note that these last two terms are antisymmetric around the z axis, and their contributions vanish when the detector polarizer is parallel to or perpendicular to the z axis. That is when there is symmetry around the atomic beam axis.

The fundamental cross sections of Sec. III A provide a quantitative interpretation of the alignment effects in terms of the magnetic sublevels of the colliding atoms. The fit parameters of Secs. III B and III C, on the other hand, are the values that are actually measured in the laboratory. These fit parameters are linearly related to the fundamental cross sections, but have no intuitive interpretation beyond that of Eqs. (14), (17), and (18). The explicit relationships between the fit parameters and the fundamental cross sections are given in Appendix B. Much of the rest of this paper describes the details of the experimental method by which the fit parameters are obtained. Once all of the fit parameters have been obtained, they are converted into the more physical fundamental cross sections by solving the equations in Appendix B.

Taking Eq. (19) into account, there are 15 independent parameters that can be obtained in these experiments. In reality, since relative signals are always measured, the actual measured quantities will always be ratios of these parameters. The net effect is that we first measure 14 values relative to one another. In Sec. V, four more values will be measured. This is still far short of the 39 parameters needed to fully describe the alignment effects of the Ca energy-pooling process. In order to get all 39 possible parameters, we could, for example, prepare two circularly polarized states with the symmetry axis 45° off of the z axis and a 45° azimuthal angle between the two states. This is beyond the scope of the present experiments.

IV. FINAL-STATE POLARIZATION RESULTS

A. Experimental procedure

As indicated above, these experiments are performed with a constant magnetic field directed parallel to the x axis. In the case of linearly polarized initial-state excitation, the laser is

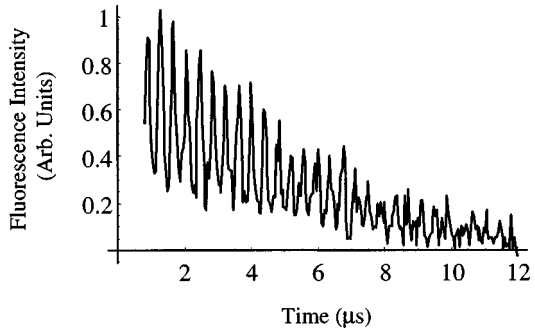

FIG. 3. An example of the final-state fluorescence intensity plotted as a function of time. Large modulations in the energy-pooling cross section are seen as the initial electronic states precess in the magnetic field, which is directed along the x axis. Here circularly polarized excitation is used and the detector polarizer is set at $\theta = 45°$.

polarized parallel to the z axis, and in the case of circular excitation, the laser is polarized around the y axis. The angle between the symmetry vector and the z axis changes periodically, resulting in a modulation of the energy-pooling cross section. A polarizer is placed between the detector and the collision region. The resulting signal is described by Eqs. (17) and (18) and is a function of both $\beta\ (=\omega t)$, the angle between the symmetry vector of the colliding atoms and the z axis, as well as θ, the angle between the detector polarizer and the z axis. The z axis is parallel to the atomic beam axis and thus parallel to the relative velocity vector of the collisions.

Figure 3 shows an example of the raw data with the detector polarizer set at about 45° to the z axis when circularly polarized excitation is used. Not surprisingly, the signal looks very similar to the data obtained in Parks *et al.*, when the detector polarizer was not used. The signal here is much noisier than in the earlier report because the fluorescence collection angle is much smaller and the polarizer further reduces the signal. Recall that the condenser lens is not used to collect the fluorescence here because it alters the polarization of the light. In a full data run, the polarizer is rotated 180° and then rotated back to the starting point in 15° steps. At each 15° step the signal as a function of time is averaged over 1000 laser pulses. The data is averaged over the time range (10 μs), and greater weight is given to earlier times in the analysis, when the signal strength is largest. This time range means that the results represent the alignment effects averaged over a velocity distribution with a mean of 400 m/s and a full width at half maximum of 460 m/s.

B. Results

1. Change in the mean signal (averaged over the modulations due to magnetic precession) as the detector polarizer is rotated

First we examine how the mean signal, averaged over the modulation due to the magnetic precession, varies as the detector polarizer is rotated. Some of the results are shown in Fig. 4 for both linear and circular excitation. The variation versus θ is distinct and very similar for both cases. The signal is greatest when the axis of the detector polarizer is parallel to the z axis and decreases to about 60% of this value

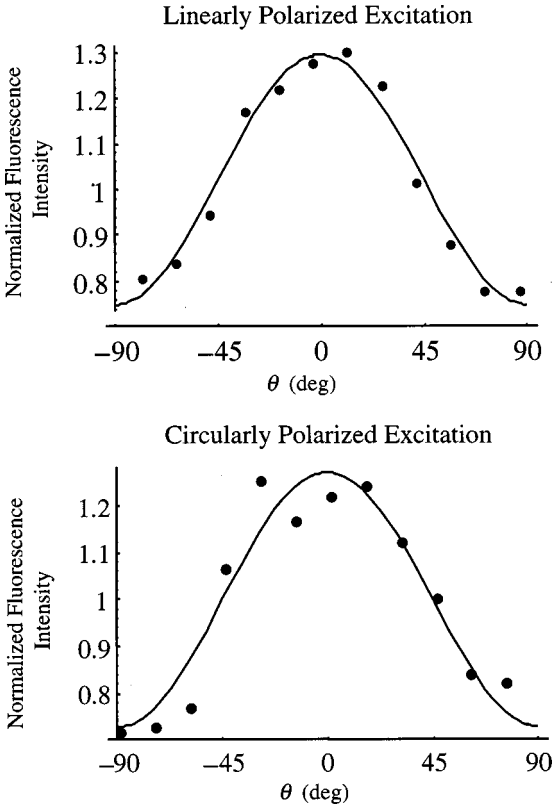

FIG. 4. The signal averaged over the modulations due to magnetic precession plotted as a function of the detector polarizer angle θ. Both of these curves have been normalized so that the mean value is 1. The top plot shows the signal when linearly polarized excitation is used, and circularly polarized excitation is used in the bottom plot.

when y-polarized fluorescence is observed. The signals shown in Fig. 4 have been normalized so that the average signal in each case is one. The fit in Fig. 4 is thus to the form

$$I(\theta) = 1 + \frac{l_{l,c}}{k_{l,c}} \cos(2\theta). \tag{21}$$

This simply uses Eqs. (17) and (18) averaged over ωt and divided by the mean signal strength. For the case of linear polarization the amplitude of the modulation is $l_l/k_l = 0.254 \pm 0.019$ and for the case of circular polarization, $l_c/k_c = 0.246 \pm 0.021$. There is no expectation that the modulation is the same for the linear and circular cases, but this is what the data determines. In order to rule out artifacts, the initial-state fluorescence was separately observed through the detector polarizer, and no preference for z-polarized fluorescence was observed.

2. Modulations due to magnetic precession averaged over θ

The parameters $d_{l,c}/k_{l,c}$ and $g_{l,c}/k_{l,c}$ from Eqs. (17) and (18) describe when the signal is averaged over all values of θ. These values were found in A, and when averaged over the velocity distribution of this experiment they are $d_l/k_l = 0.117 \pm 0.006$, $g_l/k_l = 0.054 \pm 0.007$, $d_c/k_c = -0.56 \pm 0.01$, and $g_c/k_c = 0.081 \pm 0.009$.

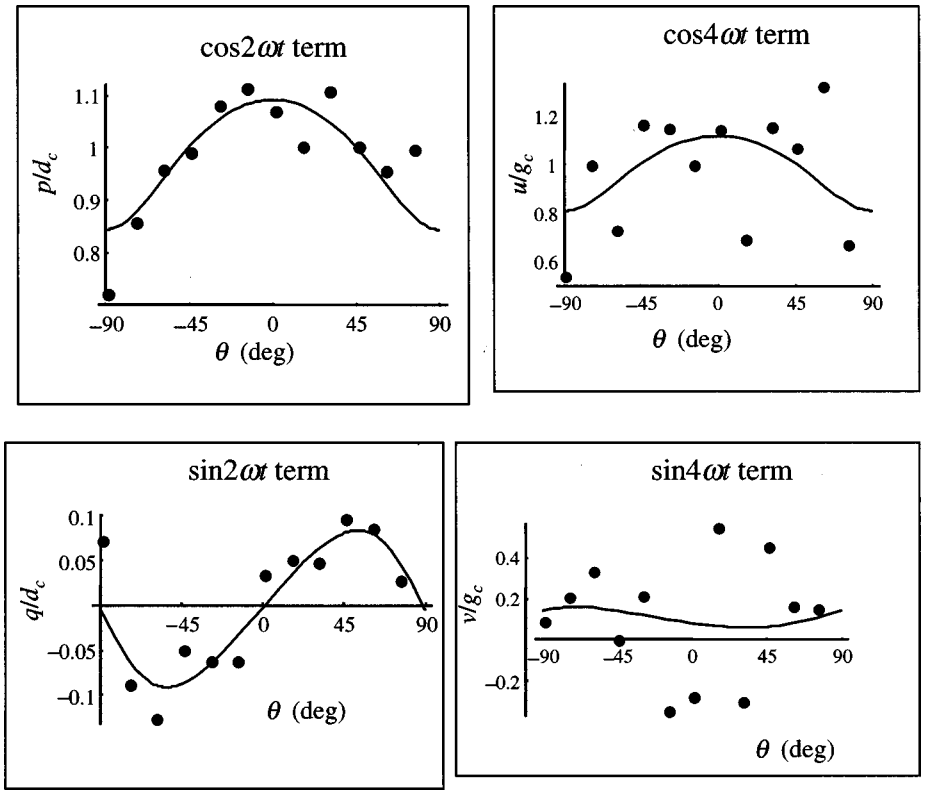

FIG. 5. The parameters p, q, u, and ν, in the case of circularly polarized excitation plotted as a function of the detector polarizer angle, θ. These parameters describe the modulation in the signal due to the magnetic precession, which has the form $p\cos 2\omega t + q\sin 2\omega t + u\cos 4\omega t + \nu \sin 4\omega t + 1$. The fits are described in the text.

3. Change in the modulations due to magnetic precession as the detector polarizer is rotated

Next consider the parameters $e_{l,c}$, $h_{l,c}$, $f_{l,c}$, and $j_{l,c}$. These parameters describe how the modulation due to the magnetic precession changes as the detector polarizer is rotated. To find these parameters, the signal as a function of time must be fit at each angle of θ. As in Parks *et al.*, the long-time decay is removed by dividing the signal by its value averaged over one modulation period. The form of the signal as a function of time can be then written, for both linearly and circularly polarized excitation:

$$I(t) = p\cos 2\omega t + q\sin 2\omega t + u\cos 4\omega t + \nu\sin 4\omega t + 1, \tag{22}$$

where the parameters p, q, u, and ν depend on θ.

By comparing Eq. (21) with Eqs. (17) and (18), and knowing that the divisor, when the long-time decay is removed, is the value of the signal when averaged over the time modulations, or $k_{l,c} + l_{l,c}\cos 2\theta$, the result is

$$p_{l,c} = \frac{d_{l,c} + e_{l,c}\cos 2\theta}{k_{l,c} + l_{l,c}\cos 2\theta}, \quad q_{l,c} = \frac{a + f_{l,c}\sin 2\theta}{k_{l,c} + l_{l,c}\cos 2\theta},$$

$$u_{l,c} = \frac{g_{l,c} + h_{l,c}\cos 2\theta}{k_{l,c} + l_{l,c}\cos 2\theta}, \quad \nu_{l,c} = \frac{b + j_{l,c}\sin 2\theta}{k_{l,c} + l_{l,c}\cos 2\theta}. \tag{23}$$

The parameters a and b are used to compensate for any error in the time origin. The values $l_{l,c}/k_{l,c}$, $d_{l,c}/k_{l,c}$, and $g_{l,c}/k_{l,c}$ have already been obtained above. It is convenient to divide $p_{l,c}$ and $q_{l,c}$ by $d_{l,c}/k_{l,c}$ and $u_{l,c}$, and to divide $\nu_{l,c}$ by $g_{l,c}/k_{l,}$. The result is

$$\frac{p_{l,c}}{d_{l,c}/k_{l,c}} = \frac{1 + \dfrac{e_{l,c}}{d_{l,c}}\cos 2\theta}{1 + \dfrac{l_{l,c}}{k_{l,c}}\cos 2\theta}, \quad \frac{q_{l,c}}{d_{l,c}/k_{l,c}} = \frac{a + \dfrac{f_{l,c}}{d_{l,c}}\sin 2\theta}{1 + \dfrac{l_{l,c}}{k_{l,c}}\cos 2\theta},$$

$$\frac{u_{l,c}}{g_{l,c}/k_{l,c}} = \frac{1 + \dfrac{h_{l,c}}{g_{l,c}}\cos 2\theta}{1 + \dfrac{l_{l,c}}{k_{l,c}}\cos 2\theta}, \quad \frac{\nu_{l,c}}{g_{l,c}/k_{l,c}} = \frac{b + \dfrac{j_{l,c}}{g_{l,c}}\sin 2\theta}{1 + \dfrac{l_{l,c}}{k_{l,c}}\cos 2\theta}. \tag{24}$$

The fitting procedure is as follows. The signal as a function of time for each value of θ is fitted to Eq. (22) to find p, q, u, and ν. These parameters are then divided by $d_{l,c}/k_{l,c}$ or $g_{l,c}/k_{l,c}$. This gives the quantities $p_{l,c}/(d_{l,c}/k_{l,c})$, $q_{l,c}/(d_{l,c}/k_{l,c})$, $u_{l,c}/(g_{l,c}/k_{l,c})$, and $\nu_{l,c}/(g_{l,c}/k_{l,c})$ as a function of θ. These parameters are then fit to the form of Eq. (24). An example of the data obtained with circularly polarized excitation is shown in Fig. 5. Here the values $p_c/(d_c/k_c)$, $q_c/(d_c/k_c)$, $u_c/(g_c/k_c)$, and $\nu_c/(g_c/k_c)$ are plotted as function of θ. These values are the normalized coefficients in front of the $\cos 2\omega t$, $\sin 2\omega t$, $\cos 4\omega t$, and $\sin 4\omega t$ terms, respectively, in Eqs. (17) and (18). There is clearly a modulation in the $\cos 2\omega t$ and $\sin 2\omega t$ terms $[p_c/(d_c/k_c)$ and $q_c/(g_c/k_c)]$. This modulation is symmetric around the beam axis for the $\cos 2\omega t$ term and antisymmetric for the $\sin 2\omega t$ term. Also the $\cos 2\omega t$ term is about 20% smaller when the detector polarizer is perpendicular to the atomic-beam axis than when the detector polarizer is parallel to the beam axis. The data for the $\cos 4\omega t$ and $\sin 4\omega t$ terms $[u_c/(g_c/k_c)$ and $\nu_c/(g_c/k_c)]$ are not as clear. There is some modulation, barely detectable over the noise, in the $\cos 4\omega t$

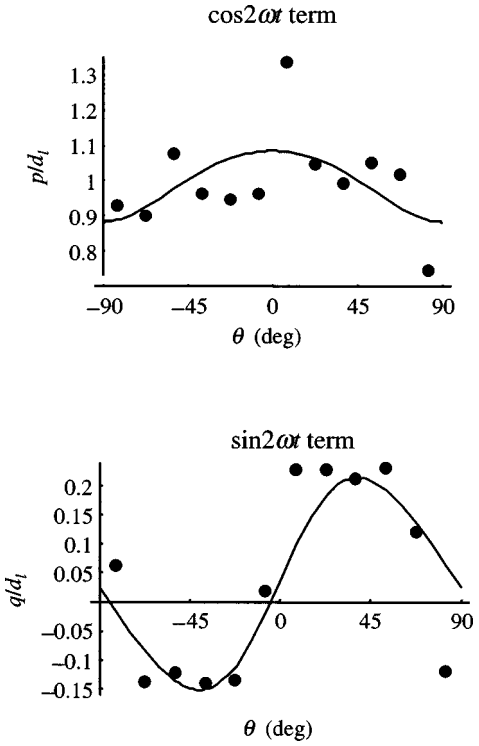

FIG. 6. The parameters p and q plotted as a function of θ for linearly polarized excitation. The signal, as the atoms precess in the magnetic field, has the form $p\cos 2\omega t+q\sin 2\omega t+u\cos 4\omega t+v\sin 4\omega t+1$. In the linear case no θ dependence can be seen above the noise for the parameters u and v.

term, but no detectable modulation in the $\sin 4\omega t$ term. The data shown in Fig. 5 gives $e_c/d_c=0.39\pm0.03$, $f_c/d_c=0.08\pm0.01$, $h_c/g_c=0.4\pm0.1$, and $j_c/g_c=0.04\pm0.10$. Some of the data for the $\cos 2\omega t$ and $\cos 2\omega t$ terms of the linearly polarized excitation case are shown in Fig. 6. The result is less obvious here, but there is definitely some modulation. For linear polarization, the results are $e_l/d_l=0.30\pm0.04$, $f_l/d_l=0.18\pm0.03$, and $h_l/g_l=0.12\pm0.10$, $j_l/g_l=0.07\pm0.10$.

The sum $p\cos 2\beta+q\sin 2\beta$, which describes the signal as the symmetry axis rotates with the polarizer set at a particular θ, can be expressed as a $\cos 2\beta$ term with the maximum shifted from $\beta=0$. Here ωt has been replaced by β to emphasize that this quantity is the angle between the symmetry axis of the atom and the z axis. When the detector polarizer is aligned with the z axis, the maximum is at $\beta=0$. This is not surprising because of the symmetry around the z axis in this case. But as the detector polarizer is rotated off the z axis the signal is no longer constrained to be symmetric about $\beta=0$. Thus the maximum of the quantity $p\cos 2\beta+q\cos 2\beta$ can, and does, move off of the z axis. In this experiment, it is found that the maximum point of the signal rotates in the same direction as the detector polarizer. The maximum continues moving in the direction of the detector polarizer until $\theta=45°$. As the angle of the detector polarizer increases still further the signal maximum moves back towards the z axis, and symmetry about the z axis is again restored when $\theta=90°$. This is true for both linearly and circularly polarized excitation. When the detector polarizer is at $\theta=45°$, the maximum is shifted away from the beam axis by the maximum amount, 5° for linear excitation and 3° for circular excitation.

All of the parameters defined in Eqs. (17) and (18) have now been determined. The signal modulation as the initial-state atoms precess in the applied magnetic field has a weak dependence on the detector polarizer angle. The modulations due to the magnetic precession change by only about 10% as the detector polarizer is rotated. There is, however, a 40% decrease in the average signal as the detector polarizer is rotated from parallel to the z axis to perpendicular to the z axis. This is true when both linearly and circularly polarized initial-state excitation is used.

C. Uncertainties

The assignment of uncertainties to $d_{l,c}/k_{l,c}$ and $g_{l,c}/k_{l,c}$ has been discussed in Parks *et al.* and the uncertainties in $n_{l,c}/m_{l,c}$ were discussed in Sec. III. Experimental noise is the main source of error in the rest of the parameters. Because there is such a small collection angle for the fluorescence, long integration times must be used. It takes nearly 20 minutes to sweep the final-state polarizer 180° in 15° steps. During this time the Ca beam flux, as well as the laser tuning and power may change, resulting in the noise level in Fig. 4. In addition, the low signal strengths make it difficult to fit the modulation signals produced by the magnetic precession.

Radiation trapping is another possible source of error. The polarization of the final-state fluorescence could be altered if it is absorbed and re-emitted before it leaves the interaction region. Since the energy-pooling process is highly exothermic, the Ca atoms leave the collision at a velocity of over 1300 m/s. This corresponds to a Doppler shift of 3 GHz, much larger than the 200-MHz natural-line width of the $4s^2\ {}^1S_0\rightarrow 4s4p\ {}^1P_1$ transition and the 300-MHz Doppler width of the atomic beam. Thus it is unlikely that a final-state photon will be absorbed by another Ca atom before it reaches the detector. In order to test for radiation trapping, the oven temperature was decreased from 1020 to 930 K resulting in a factor of 2 decrease in Ca density in the interaction region. The signal strength with linearly polarized excitation, averaged over the magnetic precession, was measured with the detector polarizer first parallel, then perpendicular, to the z axis. The result is that l_l/k_l (930 K) $=0.28\pm0.06$, which agrees well with the value at 1020 K, l_l/k_l (1020 K) $=0.254\pm0.019$. Thus we conclude that radiation trapping does not have a large effect on these results.

V. THE APPLICATION OF A MAGNETIC FIELD GRADIENT

A. Theory

The experiments described thus far involve two initial-state atoms colliding with the same alignment. More alignment information can be obtained by studying collisions between atoms that do not have parallel alignments. One obvious way to do this is to excite the initial-state atoms with two laser beams, each with a different polarization. With this method the exact population of the excited-state atoms produced by each laser beam must be known. This will not be simple if the laser beams are not perfectly overlapped and if the pumping transitions are approaching saturation. A differ-

ent approach is used here. A magnetic-field gradient is applied, with both the direction of the magnetic field and the direction of the gradient parallel to the atomic beam axis. When linear polarization is used, the laser is now polarized along the x axis instead of the z axis as in the previous sections. When circular polarization is used, the laser is still polarized around the y axis. Since the collisions occur with faster atoms catching up to slower atoms, the collisions in time occur between atoms that have experienced different amounts of magnetic precession. So collisions between nonparallel orbitals are realized.

With the magnetic gradient switched off, collisions only occur between atoms with parallel symmetry axes. If $\Delta\alpha$ denotes the azimuthal angle between the symmetry axes of the two atoms, then $\Delta\alpha=0$ when the gradient is switched off. However, with the field gradient present, the observed signal is averaged over collisions with all values of $\Delta\alpha$. To understand how this works, an experiment is discussed in more detail. Consider an orbital that is initially in a p_x state and then has been rotated by an angle α_1 around the z axis. If this atom collides with another atom that is initially in a p_x state that has then been rotated by an angle α_2 around the z axis, the experimentally observed energy-pooling cross section is

$$\sigma_{\mathrm{exp}}=\tfrac{1}{2}(\sigma_{1-10}+\sigma_{1-10;-110}\cos\Delta\alpha+\sigma_{110}), \qquad (25)$$

where $\Delta\alpha$ is equal to the difference between α_1 and α_2.

First, if the p_x orbitals are in a weak uniform magnetic field of strength B_0 directed along the z axis, the atoms will precess at a rate ω so that at any time t, $\alpha_1=\alpha_2=\omega t$. Explicitly this is

$$\alpha_1=\alpha_2=\frac{\mu_B B_0 g t}{\hbar} \qquad (26)$$

and $\Delta\alpha=0$ always. Now consider a system with a magnetic field described by $\mathbf{z}(B_0+zs)$, where s is a constant. We will assume that the gradient s is small enough so that it has a negligible effect on the motion of the atoms. Then $\Delta\alpha(t)$ can be found by integrating Eq. (26) for each atom over the magnetic field experienced by each atom before the collision. Take v_1 and v_2 to be the velocity of the two atoms. Take the collision to occur at time t and at position $z=0$. Atom one has moved from $z=-v_1 t$ at $t=0$ to $z=0$ at t. The average magnetic field that is felt by this atom is $B_0-v_1 ts/2$. Therefore, $\alpha_1(t)=t\mu_B g(B_0-v_1 ts/2)/\hbar$. The same is true for atom two, so

$$\Delta\alpha=\frac{(v_1-v_2)\mu_B g s t^2}{2\hbar}. \qquad (27)$$

Thus,

$$\sigma_{\mathrm{exp}}=\tfrac{1}{2}\left\{\sigma_{1-10}+\sigma_{1-10;-110}\cos\left[\frac{(v_1-v_2)\mu_B g s t^2}{\hbar}\right]+\sigma_{110}\right\}, \qquad (28)$$

The contribution from the coherence term oscillates in time. Finally, to obtain the experimentally observed signal, Eq. (28) must be integrated over the velocity distribution of the atomic beam. The result of the integration over the broad velocity distribution of the beam is that the oscillation of Eq. (28) quickly averages to zero. A model result of this integration for the coherence term is plotted in Fig. 7, assuming that the cross sections are independent of the collision velocity. Also, the collision velocity is taken to be the relative velocity of the beam given by Eq. (1). Actually, the situation is slightly more complicated than this. As seen in Parks *et al.*, the fundamental cross sections do depend on velocity, and the collision velocity distribution is time dependent. However, the rough form of the experimental data will still look quite similar to Fig. 7.

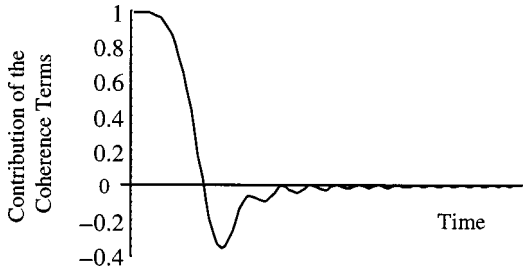

FIG. 7. The contribution of the coherence terms to the total signal when a magnetic-field gradient is applied. Due to the broad velocity distribution in the Ca beam, the coherence terms quickly average to zero.

Only the contribution of the coherence term to the total cross section is shown in Fig. 7. To get the actual cross section, this must be added to the contribution of the conventional terms, which are not affected by the magnetic gradient. In effect, the magnetic-field gradient allows the coherence terms to be switched off by randomizing the azimuthal angles of the colliding atoms, leaving only the conventional cross sections. In the basis that is used, all of the azimuthal information is contained in phase information. The ratio of the signal at long times, when the contribution from the coherence term has gone to zero, to the signal at $t=0$ is $(\sigma_{1-10}+\sigma_{1-10;-110}+\sigma_{110})/(\sigma_{1-10}+\sigma_{110})$. This ratio will be denoted by z_l. The values of $\sigma_{1-10}+\sigma_{1-10;-110}$ and σ_{110} have already been measured in the experiments described in the last section. Now the separate values of all three cross sections can be obtained. This experiment can be repeated with the detector polarizer perpendicular to the z axis, giving a parameter y_l. This parameter is a ratio of more complicated sums of the fundamental cross sections, obtained for σ_{exp} from Eq. (2). Then the parameter y_l can be found by taking the ratio of $\int_0^{2\pi}\sigma_{\mathrm{exp}}(\Delta\alpha)d\alpha$ and $\sigma_{\mathrm{exp}}(\Delta\alpha=0)$. This can be repeated with circularly polarized excitation to get the parameters y_c and z_c.

B. Experiment

The experiment is performed by first switching on the magnetic-field gradient and averaging 1000 laser pulses with the detector aligned parallel to the z and then the y axes. Then the gradient field is switched off leaving a constant magnetic field of 0.2 Gauss directed along the z axis. The signal, averaged over 1000 laser pulses, is again recorded with the polarizer directed along the y then the z axes. In the circular case the strength of the gradient is $dB/dz=1.5$ G/cm and the average value of B in the interaction region is 7 G. In the linear case $dB/dz=0.75$ G/cm and the average value of B is 3.5 G.

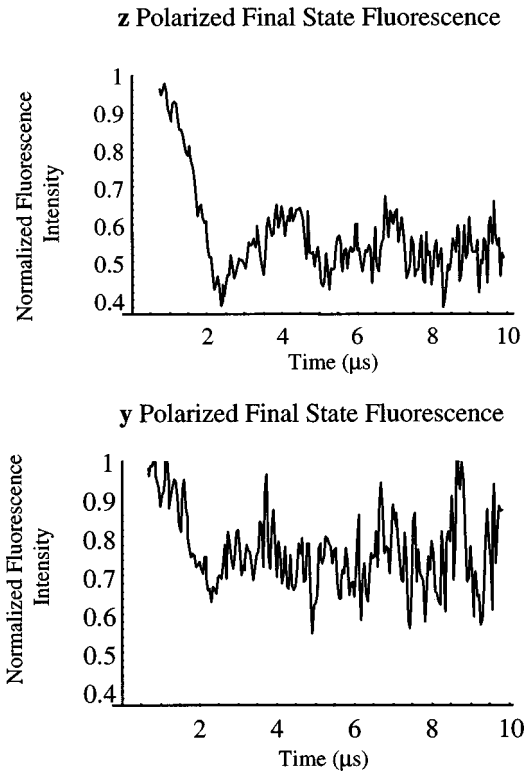

FIG. 8. These plots show the signal as a function of time with the magnetic-field gradient present divided by the signal with the gradient turned off. Linearly polarized excitation is used here. In the top plot the detector polarizer is oriented parallel to the z axis, and in the bottom plot the polarizer is perpendicular to this. Since the coherence terms are positive here, the signal decreases when the gradient is applied. Notice that the signal does not drop as much in the y-polarized case as in the z-polarized case.

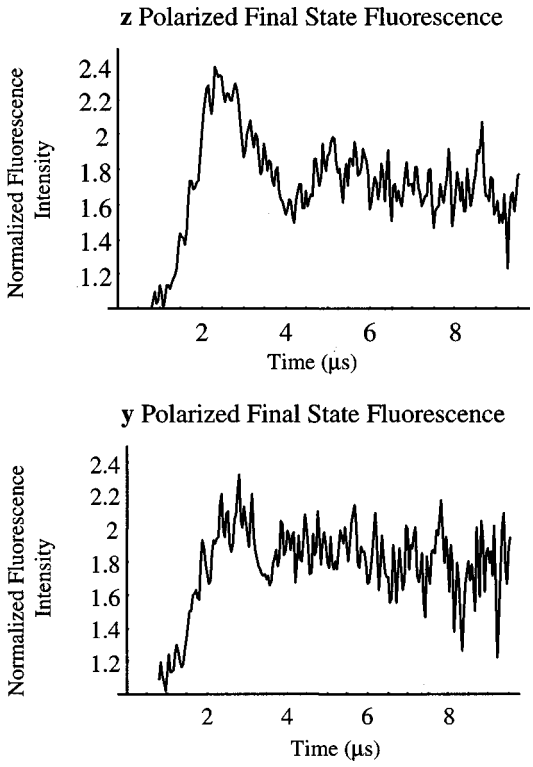

FIG. 9. Shown here is the signal as a function of time with the magnetic-field gradient present divided by the signal with the gradient turned off for the circularly polarized excitation. In the top plot the detector polarizer is oriented parallel to the z axis, and in the bottom plot the polarizer is perpendicular to this. The signal increases when the gradient is applied because the dominant coherence terms in this case are negative.

In order to remove the long-term decay seen in all of the signals, the signal with the gradient switched on is divided by the signal with the gradient switched off for each of the above cases. The data for the case of linear laser polarization is shown in Fig. 8. The experimental data looks similar to the predicted form shown in Fig. 7. The signal decreases sharply, and one oscillation can be seen before the signal goes to roughly a constant value. The data gets noisier as time progresses because of the long-time decay of the signal. This decay has been divided out, but this means that the noise gets relatively larger for longer times. The top plot corresponds to the experiment described in detail in Sec. V A. Since σ_{110} is small (about 6% of the value of $\sigma_{1-10}+\sigma_{1-10;-110}$), the fact that the signal with the gradient turned on decreases to 50% of the value with the gradient off means that $\sigma_{1-10}\approx\sigma_{1-10;-110}$. In fact, the parity rule given in Eq. (11) means that these two cross sections must be equal. Thus the corresponding parameter z_l does not really give any new information. However, no such relation exists in the y-polarized case, and the parameter y_l is truly a new parameter. Notice that the signal does not decrease as much here. The parameters z_l and y_l are obtained from the data in Fig. 8 by taking the average value of the signal between 4.5 and 8 μs. These values are $z_l=0.55\pm0.07$ and $y_l=0.74\pm0.07$.

The data for the case of circularly polarized excitation is shown in Fig. 9. Here the coherence terms turn out to be negative, so the signal increases when the magnetic gradient is switched on. The values obtained from this data are $z_c=1.69\pm0.16$ and $y_c=1.81\pm0.18$. The magnetic gradient used here has twice the magnitude as the gradient used for the case of linearly polarized excitation. However, the signal here evolves over the same time scale as in the linear case, not twice as fast. This is because in the linear case, the state returns to itself when rotated by 180° (except for a global phase factor), while in the circular case the state must be rotated by a full 360° in order to return to the starting point. The signal with the gradient switched off was smoothed before it was used as the divisor to make these plots. This is significant, because, as seen in Sec. III, there are some modulations in this signal due to the alignment of the final state, which would be seen in the data if they were not removed.

VI. RESULTS AND DISCUSSION

We have measured 18 of the 39 independent fit parameters needed to completely describe the alignment effects in Ca energy pooling. Each of these parameters is equal to a sum of the fundamental cross sections, as given in Appendix B. These equations can be inverted, giving fundamental cross sections in terms of the measured fit parameters. If we were able to measure all 39 fit parameters, we could determine all 39 of the fundamental cross sections. However, since not all of the possible alignment information has been extracted in these experiments, not all fundamental cross sec-

TABLE I. Values of the four vector fundamental cross sections.

Fundamental cross section	Measured Value
σ_{000}	1.47 ± 0.04
σ_{001}	0.87 ± 0.03
σ_{110}	0.124 ± 0.014
$\frac{1}{2}(\sigma_{111}+\sigma_{11-1})$	0.098 ± 0.011
σ_{010}	0.51 ± 0.16
$\sigma_{010;100}$	-0.17 ± 0.17
$\frac{1}{2}(\sigma_{01-1}+\sigma_{011})$	0.13 ± 0.11
σ_{1-10}	1.15 ± 0.15
σ_{1-11}	0.95 ± 0.11
$\sigma_{1-11;-111}$	0.37 ± 0.10
$\mathrm{Re}\,\sigma_{000;1-10}$	-0.73 ± 0.04
$\mathrm{Re}\,\sigma_{1-1-1;111}$	0.00 ± 0.01
$2\,\mathrm{Re}\,\sigma_{001;1-11}+\sigma_{01-1;10-1}+\sigma_{011;101}$	-0.92 ± 0.18
$\sigma_{011}-2\,\mathrm{Re}\,\sigma_{001;1-11}+\sigma_{011;101}$	0.89 ± 0.05
$\frac{1}{2}\,\mathrm{Re}\,\sigma_{001;-1-1-1}+2\,\mathrm{Re}\,\sigma_{001;1-11}+\frac{1}{2}\,\mathrm{Re}\,\sigma_{00-1;111}$	-1.00 ± 0.08
$\mathrm{Re}\,\sigma_{-100;-111}+\mathrm{Re}\,\sigma_{0-10;-111}-2\,\mathrm{Re}\,\sigma_{1-10;011}$	0.011 ± 0.015
$\mathrm{Re}\,\sigma_{-100;001}-\mathrm{Re}\,\sigma_{000;011}$	-0.029 ± 0.007
$\mathrm{Re}\,\sigma_{-1-10;-101}-\mathrm{Re}\,\sigma_{010;111}$	-0.017 ± 0.005

tions are solved for individually. The results are given in Table I, where the relative values of 18 fundamental cross sections or sums of cross sections are reported. The alignment effects are large and distinct. The conventional cross sections σ_{110}, $\frac{1}{2}(\sigma_{111}+\sigma_{11-1})$, and $\frac{1}{2}(\sigma_{011}+\sigma_{01-1})$ are over an order of magnitude smaller than the largest conventional cross section σ_{000}. Also, the cross sections with a final $m_j=0$ state are generally larger than the cross sections that form the $m_j=\pm1$ states. The cross section σ_{010} is several times larger than $\frac{1}{2}(\sigma_{011}+\sigma_{01-1})$, while σ_{000} is one and a half times larger than σ_{001}. As for the coherence terms, sums containing the cross sections $\mathrm{Re}\,\sigma_{000;1-10}$ and $\mathrm{Re}\,\sigma_{001;1-11}$ have large negative values (the exception is the sum $\sigma_{011}-2\,\mathrm{Re}\,\sigma_{001;1-11}-\sigma_{010;101}$, where $\mathrm{Re}\,\sigma_{001;1-11}$ has a minus sign). The cross section $\sigma_{1-11;-111}$ has a small but distinct positive value. As shown in Sec. V, the coherence term $\sigma_{1-10;-110}$ is constrained to be equal to σ_{1-10}, which is large and positive. In addition, it was seen in Sec. IV that when the initial states are precessing, small $\sin2\omega t$ and $\sin4\omega t$ terms appear if the final-state polarization is resolved. This effect is described here by the small but nonzero values for $\mathrm{Re}\,\sigma_{-100;001}-\mathrm{Re}\,\sigma_{000;011}$ and $\mathrm{Re}\,\sigma_{-1-10;-101}-\mathrm{Re}\,\sigma_{010;111}$.

A complete explanation of these alignment results is likely to be quite complicated. Models involving single or multiple curve crossings are often invoked to explain alignment effects in atomic collisions. A few of the many examples of this include work on $\mathrm{Ca}(^1F)+\mathrm{He}$ [22] and Na+He [23,24] inelastic collisions, as well as the theoretical models of the $\mathrm{Na}(3p)+\mathrm{Na}(3p)$ system [25–27]. In the $\mathrm{Ca}(^3P)+\mathrm{Ca}(^3P)$ case, the situation is complicated by the large number of states involved. While there are only three molecular states, which correspond to the $^1P+{}^1S$ final state, there are 18 molecular states that correlate with the $^3P+{}^3P$ initial state. None of the Ca-Ca curves relevant to this experiment have been published, although a few of the curves in the analogous Sr-Sr system do exist [28].

A more important complication is spin-orbit coupling. Most of the previous theoretical work has focused on states with no spin, such as the Ca+He work. In the case of the $\mathrm{Na}(3p)+\mathrm{Na}(3p)$ work, states with spin are involved but the models assume that the spin-orbit coupling is too weak to affect the alignment on the collision time scale. However, this condition is not met in the $\mathrm{Ca}(^3P)+\mathrm{Ca}(^3P)$ case. The spin-orbit precession period of Ca is 1×10^{-13} s. At the average collision velocity of these experiments, the Ca atoms will only move a distance of one bohr (a_0) in this time. In the Sr-Sr system, the $^3P+{}^3P$ and the $^1P+{}^1S$ curve crossing occurs at an internuclear separation near $10a_0$ and the atoms may interact significantly at separations of greater than $50a_0$, if this system is anything like the $\mathrm{Na}(3p)+\mathrm{Na}(3p)$ system that has been theoretically studied [27]. Thus the effects of spin-orbit coupling will have to be taken into account. Despite over ten years of work on the $\mathrm{Na}(3p)+\mathrm{Na}(3p)$ collision data, no theory yet takes into account the weaker spin-orbit effects in this system [25–27]. All $\mathrm{Na}(3p)+\mathrm{Na}(3p)$ calculations apply only to high-collision velocities where spin-orbit coupling can be neglected. However, the fact that such large polarization effects are observed indicates that important general principles are likely to be uncovered by a careful theoretical analysis of this system.

VII. CONCLUSION

In this paper, we have carried out a type of four-vector experiment, where two aligned atoms are collided and the alignment of one of the final states is partially resolved. To our knowledge, the detailed information obtained in this four-vector experiment is unprecedented. In Parks *et al.* it was found that the energy-pooling cross section is strongly dependent on the initial-state alignment. Here it is found that the final state is produced with an alignment predominantly along the relative velocity vector of the collision. This final-state alignment is only weakly correlated with the initial-state alignment. Furthermore, we have shown that a magnetic gradient can be used to turn off the interference terms and thus obtain additional alignment information. A complete explanation for the data goes well beyond the remarks here. Describing the dynamics of this type of collision will be a very stringent test of theory.

ACKNOWLEDGMENT

The authors gratefully acknowledge support by the National Science Foundation.

APPENDIX A

Following Arthurs and Dalgarno [20], consider a partial-wave expansion of the scattering amplitudes. Arthurs and Dalgarno deal only with a rigid rotor colliding with a structureless atom. This is extended to the case of two identical atoms colliding here. The amplitude for two atoms initially in magnetic states m_1 and m_2 to scatter into a final state with the excited-state atom in a magnetic substate m_3 can be written

$$f_{jm\lambda_f m'}(\theta,\varphi)=\sum_{\substack{j'',m_l'',J,\\ l,l',M}}\frac{(-1)^{j+j'}i^{l-l'+1}\sqrt{\pi}\sqrt{2l+1}(2J+1)}{\sqrt{k_ik_f}}\times\begin{pmatrix} j & l & J\\ m & 0 & -M\end{pmatrix}\begin{pmatrix} j'' & l'' & J\\ m_3 & m_l'' & -M\end{pmatrix}\times T^J_{jl\lambda;j''l''\lambda_f}Y_{l''m_l''}(\theta,\varphi). \tag{A1}$$

Here j and j' represent the total angular momenta before and after the collision, respectively. The orbital angular momenta before and after the collision are given by l and l'', respectively. Also m_l'' is the magnetic quantum number corresponding to l''. J and M represent the total (electronic plus orbital) angular momentum of the colliding system. In addition, $m\equiv m_1+m_2$. The symbols λ_i and λ_f represent all of the other quantum numbers needed to specify the initial and final atomic states, respectively. $T^J_{jl;l'}$ is the transition matrix, and the initial- and final-state wave vectors are k_i and k_f, respectively Finally, the scattering angles are represented by φ and θ. Equation (A1) is nearly identical to the equation derived by Arthurs and Dalgarno [20], except that now j represents the coupled electronic angular momenta of both colliding atoms before the collision. It is more useful to express the scattering amplitudes in terms of m_1 and m_2 instead of j and m. To do this, we must construct a superposition of states with different j's to describe an (m_1,m_2) state. Thus, we get

$$f_{m_1m_2\lambda_f m_3}(\theta,\varphi)=\frac{1}{\sqrt{k_ik_f}}\sum_{\substack{j,j',m_l',\\ J,l,l',M}}i^{l-l'+1}(-1)^{j+j'+j_1-j_2-m}\times\sqrt{\pi}\sqrt{2l+1}(2J+1)T^J_{jl\lambda_i;j'l'\lambda_f}\times Y_{l'm_l'}(\theta,\varphi)\begin{pmatrix} j & l & J\\ m & 0 & -M\end{pmatrix}\times\begin{pmatrix} j' & l' & J\\ m_3 & m_l' & -M\end{pmatrix}\begin{pmatrix} j_1 & j_2 & j\\ m_1 & m_2 & -m\end{pmatrix}. \tag{A2}$$

Since the bottom rows of the $3j$ symbols must add to zero, we have $m=m_1+m_2$, $M=m_1+m_2$, and $m_l'=m_1+m_2-m_3$.

The experimentally observed cross section is found by taking the modulus squared of the scattering amplitudes, integrating over all scattering angles,

$$\begin{aligned}\sigma_{\exp}&=\frac{k_f}{k_i}\sum_{\lambda_f}\sum_{m_1,m_2}\int|a_{m_1m_2}[f_{m_1m_2\lambda_f m_3}(\theta,\varphi)+f_{m_2m_1\overline{\lambda_f}m_3}(\pi-\theta,\varphi+\pi)]|^2\sin\theta\,d\theta\,d\varphi\\&=\frac{k_f}{k_i}\sum_{\substack{m_1,m_1',\\ m_2,m_2'}}a_{m_1m_2}a^*_{m_1'm_2'}\sum_{\lambda_f,\lambda_f'}\int[f_{m_1m_2\lambda_f m_3}(\theta,\varphi)+f_{m_2m_1\overline{\lambda_f}m_3}(\pi-\theta,\varphi+\pi)][f^*_{m_1'm_2'\lambda_f'm_3}(\theta,\varphi)+f^*_{m_2'm_1'\overline{\lambda_f'}m_3}(\pi-\theta,\varphi+\pi)]\sin\theta\,d\theta\,d\varphi.\end{aligned} \tag{A3}$$

In this notation, $\overline{\lambda_f}$ gives the state λ_f with the electronic states of the two atoms switched. The fundamental cross sections are now defined as

$$\begin{aligned}\sigma_{m_1m_2m_3;m_1'm_2'm_3'}&=\frac{k_f}{k_i}\sum_{\lambda_f,\lambda_f'}\int[f_{m_1m_2\lambda_f m_3}(\theta,\varphi)+f_{m_2m_1\overline{\lambda_f}m_3}(\pi-\theta,\varphi+\pi)][f^*_{m_1'm_2'\lambda_f'm_3}(\theta,\varphi)+f^*_{m_2'm_1'\overline{\lambda_f'}m_3}(\pi-\theta,\varphi+\pi)]\sin\theta\,d\theta\,d\varphi.\end{aligned} \tag{A4}$$

Using Eq. (A2), this can be written

$$\begin{aligned}\sigma_{m_1m_2m_3;m_1'm_2'm_3'}=\frac{1}{k_i^2}\sum_{\lambda_f,\lambda_f'}\sum_{\substack{j,j',j'',j''',\\ m_l',m_l''J,J',\\ l,l'l'',l''',M,M'}}&i^{l-l'-l''-l'''}(-1)^{j+j''+j'+j'''-m-m'}\times\pi\sqrt{2l+1}\sqrt{2l''+1}(2J+1)(2J'+1)(-1)^{j_1-j_2+j_1'-j_2'}\begin{pmatrix} j & l & J\\ m_1+m_2 & 0 & -M\end{pmatrix}\begin{pmatrix} j' & l' & J\\ m_3 & m_l' & -M\end{pmatrix}\\&\times\begin{pmatrix} j_1 & j_2 & j\\ m_1 & m_2 & -m_1+m_2\end{pmatrix}\begin{pmatrix} j'' & l'' & J'\\ m_1'+m_2' & 0 & -M'\end{pmatrix}\begin{pmatrix} j''' & l''' & J'\\ m_3 & m_l'' & -M'\end{pmatrix}\begin{pmatrix} j_1' & j_2' & j''\\ m_1' & m_2' & -m_1'+m_2'\end{pmatrix}\\&\times\int[T^J_{jl\lambda_i;j'l'\lambda_f}Y_{l'm_l'}(\theta,\varphi)+(-1)^{l'}T^J_{jl\lambda_i;j'l'\overline{\lambda_f}}Y_{l'm_l'}(\theta,\varphi)][T^{J*}_{j''l''\lambda_i;j'''l'''\lambda_f'}Y^*_{l'''m_l''}(\theta,\varphi)\\&+(-1)^{l'''}T^{J*}_{j''l''\lambda_i;j'l'''\overline{\lambda_f'}}Y^*_{l'''m_l''}(\theta,\varphi)]\sin\theta\,d\theta\,d\varphi.\end{aligned} \tag{A5}$$

Upon integration over the θ and φ, the spherical harmonics can be replaced by $\delta_{l',l'''}\delta_{m_l'm_l''}$ and the result is (taking, for this experiment, $j'=j'''=j_1=j_2=1$)

$$\sigma_{m_1m_2m_3;m_1'm_2'm_3'}=\frac{1}{k_i^2}\sum_{\substack{j,j',j'',j''',\\ m_l',J,J',\\ l,l',l'',M,M'}} i^{l-l''}(-1)^{j+j''+j'+j'''-m-m'}\times\pi\sqrt{2l+1}\sqrt{2l''+1}(2J+1)(2J'+1)\times\begin{pmatrix} j & l & J\\ m_1+m_2 & 0 & -M\end{pmatrix}\times\begin{pmatrix} 1 & l' & J\\ m_3 & m_l' & -M\end{pmatrix}\begin{pmatrix} 1 & 1 & j\\ m_1 & m_2 & -M\end{pmatrix}\times\begin{pmatrix} j'' & l'' & J'\\ m_1'+m_2' & 0 & -M'\end{pmatrix}\times\begin{pmatrix} 1 & l' & J'\\ m_3' & m_l' & -M'\end{pmatrix}\times\begin{pmatrix} 1 & 1 & j''\\ m_1' & m_2' & -M'\end{pmatrix}T^I_{jl;l'}T^{J*}_{j''l'';l'}, \quad \text{(A6)}$$

where $T^J_{jl;l'}T^{J*}_{j''l'';'l'}$ represents the products of $T^J_{jl\lambda_i;j'l'\lambda_f}$ and $T^{J*}_{jl\lambda_i;j'l'\lambda_f}$ from Eq. (A1) summed over λ_f.

APPENDIX B

The equations for the fit parameters in terms of the fundamental cross sections are listed here. All of these parameters were calculated by inserting the appropriate density matrices into Eq. (2).

$$\begin{aligned} m_c=&\sigma_{-1-11;-1-11}/32+\sigma_{-101;-101}/8+\sigma_{-110;-110}/16\\ &+\sigma_{-111;-111}/16+\sigma_{-111;001}/4+\sigma_{0-11;-101}/8\\ &+\sigma_{000;-110}/4+\sigma_{000;000}/8+\sigma_{001;001}/8+\sigma_{010;010}/4\\ &+\sigma_{011;011}/8+\sigma_{1-10;-110}/16+\sigma_{1-11;-111}/16\\ &+\sigma_{100;010}/4+\sigma_{101;011}/8+\sigma_{110;110}/16+\sigma_{111;111}/32, \end{aligned} \quad \text{(B1)}$$

$$\begin{aligned} n_c=&\sigma_{-1-1-1;001}/16+\sigma_{-11-1;111}/8+\sigma_{00-1;111}/16\\ &+\sigma_{011;011}/8+\sigma_{101;011}/8, \end{aligned} \quad \text{(B2)}$$

$$\begin{aligned} k_c=&-5\sigma_{-1-1-1;001}/128+35\sigma_{-1-11;-1-11}/256\\ &+5\sigma_{-101;-101}/64-5\sigma_{-11-1;111}/64+3\sigma_{-110;-110}/128\\ &+3\sigma_{-111;-111}/128+3\sigma_{-111;001}/32+5\sigma_{0-11;-101}/64\\ &-5\sigma_{00-1;111}/128+3\sigma_{000;-110}/32+3\sigma_{000;000}/64\\ &+3\sigma_{001;001}/64+5\sigma_{010;010}/32+\sigma_{011;011}/32\\ &+3\sigma_{1-10;-110}/128+3\sigma_{1-11;-111}/128+5\sigma_{100;010}/32\\ &+\sigma_{101;011}/32+35\sigma_{110;110}/128+35\sigma_{111;111}/256, \end{aligned} \quad \text{(B3)}$$

$$\begin{aligned} l_c=&5\sigma_{-1-1-1;001}/128-35\sigma_{-1-11;-1-11}/256\\ &-5\sigma_{-101;-101}/64+5\sigma_{-11-1;111}/64+3\sigma_{-110;-110}/128\\ &-3\sigma_{-111;-111}/128-3\sigma_{-111;001}/32-5\sigma_{0-11;-101}/64\\ &+5\sigma_{00-1;111}/128+3\sigma_{000;-110}/32+3\sigma_{000;000}/64\\ &-3\sigma_{001;001}/64+5\sigma_{010;010}/32-\sigma_{011;011}/32\\ &+3\sigma_{1-1;0-110}/128-3\sigma_{1-11;-111}/128+5\sigma_{100;010}/32\\ &-\sigma_{101;011}/32+35\sigma_{110;110}/128-35\sigma_{111;111}/256, \end{aligned} \quad \text{(B4)}$$

$$\begin{aligned} d_c=&\sigma_{-1-1-;001}/32+7\sigma_{-1-11;-1-11}/64-\sigma_{-101;-101}/16\\ &+\sigma_{-11-1;111}/16-\sigma_{-110;-110}/32-\sigma_{-111;-111}/32\\ &-\sigma_{-111;001}/8-\sigma_{0-11;-101}/16+\sigma_{00-1;111}/32\\ &-\sigma_{000;-110}/8-\sigma_{000;000}/16-\sigma_{001;001}/16-\sigma_{010;010}/8\\ &-\sigma_{1-10;-110}/32-\sigma_{1-11;-111}/32-\sigma_{100;010}/8\\ &+7\sigma_{110;110}/32+7\sigma_{111;111}/64, \end{aligned} \quad \text{(B5)}$$

$$\begin{aligned} e_c=&-\sigma_{-1-1-1;001}/32-7\sigma_{-1-11;-1-11}/64+\sigma_{-101;-101}/16\\ &-\sigma_{-11-1;111}/16-\sigma_{-110;-110}/32+\sigma_{-111;-111}/32\\ &+\sigma_{-111;001}/8+\sigma_{0-11;-101}/16-\sigma_{00-11;11}/32\\ &-\sigma_{000;-110}/8-\sigma_{000;000}/16+\sigma_{001;001}/16-\sigma_{010;010}/8\\ &-\sigma_{1-10;-110}/32+\sigma_{1-11;-111}/32-\sigma_{100;010}/8\\ &+7\sigma_{110;110}/32-7\sigma_{111;111}/64, \end{aligned} \quad \text{(B6)}$$

$$\begin{aligned} g_c=&\sigma_{-1-1-1;001}/128+\sigma_{-1-11;-1-11}/256-\sigma_{-101;-101}/64\\ &+\sigma_{-11-1;111}/64+\sigma_{-110;-110}/128+\sigma_{-111;-111}/128\\ &+\sigma_{-111;001}/32-\sigma_{0-11;-101}/64+\sigma_{00-1;111}/128\\ &+\sigma_{000;-110}/32+\sigma_{000;000}/64+\sigma_{001;001}/64-\sigma_{010;010}/32\\ &-\sigma_{0110;11}/32+\sigma_{1-10;-110}/128+\sigma_{1-11;-111}/128\\ &-\sigma_{100;010}/32-\sigma_{101;011}/32+\sigma_{110;110}/128+\sigma_{111;111}/256, \end{aligned} \quad \text{(B7)}$$

$$\begin{aligned} h_c=&-\sigma_{-1-1-1;001}/128-\sigma_{-1-11;-1-11}/256+\sigma_{-101;-101}/64\\ &-\sigma_{-11-1;111}/64+\sigma_{-110;-110}/128-\sigma_{-111;-111}/128\\ &-\sigma_{-111;001}/32+\sigma_{0-11;-101}/64-\sigma_{00-1;111}/128\\ &+\sigma_{000;-110}/32+\sigma_{000;000}//64-\sigma_{001;001}/64-\sigma_{010;010}/32\\ &+\sigma_{011;011}/32+\sigma_{1-10;-110}/128-\sigma_{1-11;-111}/128\\ &-\sigma_{100;010}/32+\sigma_{101;011}/32+\sigma_{110;110}/128-\sigma_{111;111}/256, \end{aligned} \quad \text{(B8)}$$

$$\begin{aligned} k_l=&-\sigma_{-1-1-1;001}/32+3\sigma_{-1-11;-1-11}/64+\sigma_{-101;-101}/16\\ &+3\sigma_{-11-1;111}/16+3\sigma_{-110;-110}/32+3\sigma_{-111;-111}/32\\ &-\sigma_{-111;001}/8+\sigma_{0-11;-101}/16-\sigma_{00-1;111}/32 \end{aligned}$$

$$-\sigma_{000;-110}/8+3\sigma_{000;000}/16+3\sigma_{001;001}/16+\sigma_{010;010}/8+\sigma_{011;011}/8+3\sigma_{1-10;-110}/32+3\sigma_{1-11;-111}/32+\sigma_{100;010}/8\sigma_{101;011}/8+3\sigma_{110;110}/32+3\sigma_{111;111}/64, \tag{B9}$$

$$l_l=\sigma_{-1-1-1;001}/32-3\sigma_{-1-11;-1-11}/64-\sigma_{-101;-101}/16-3\sigma_{-11-1;111}/16+3\sigma_{-110;-110}/32-3\sigma_{-111;-111}/32+\sigma_{-111;001}/8-\sigma_{0-11;-101}/16+\sigma_{00-1;111}/32-\sigma_{000;-110}/8+3\sigma_{000;000}/16-3\sigma_{001;001}/16+\sigma_{010;010}/8-\sigma_{011;011}/8+3\sigma_{1-10;-110}/32-3\sigma_{1-11;-111}/32+\sigma_{100;010}/8-\sigma_{101;011}/8+3\sigma_{110;110}/32-3\sigma_{111;111}/64, \tag{B10}$$

$$d_l=-\sigma_{-1-11;-1-11}/16-\sigma_{-11;-1;111}/4-\sigma_{-110;-110}/8-\sigma_{-111;-111}/8+\sigma_{000;000}/4+\sigma_{001;001}/4-\sigma_{1-10;-110}/8-\sigma_{1-11;-111}/8-\sigma_{110;110}/8-\sigma_{111;111}/16, \tag{B11}$$

$$e_l=\sigma_{-1-11;-1-11}/16+\sigma_{-11-1;111}/4-\sigma_{-110;-110}/8+\sigma_{-111;-111}/8+\sigma_{000;000}/4-\sigma_{001;001}/4-\sigma_{1-10;-110}/8+\sigma_{1-11;-111}/8-\sigma_{110;110}/8+\sigma_{111;111}/16, \tag{B12}$$

$$g_l=\sigma_{-1-1-1;001}/32+\sigma_{-1-11;-1-11}/64-\sigma_{-101;-101}/16+\sigma_{-11-1;111}/16+\sigma_{-110;-110}/32+\sigma_{-111;-111}/32+\sigma_{-111;001}/8-\sigma_{0-11;-101}/16+\sigma_{00-1;111}/32+\sigma_{000-1;10}/8+\sigma_{000;000}/16+\sigma_{001;001}/16-\sigma_{010;010}/8-\sigma_{011;011}/8+\sigma_{1-10;-110}/32+\sigma_{1-11;-111}/32-\sigma_{100;010}/8-\sigma_{101;011}/8+\sigma_{110;110}/32+\sigma_{111;111}/64, \tag{B13}$$

$$h_l=-\sigma_{-1-1-1;001}/32-\sigma_{-1-11;-1-11}/64+\sigma_{-101;-101}/16-\sigma_{-11-1;111}/16+\sigma_{-110;-110}/32-\sigma_{-111;-111}/32-\sigma_{-111;001}/8+\sigma_{0-11;-101}/16-\sigma_{00-1;111}/32+\sigma_{000;-110}/8+\sigma_{000;000}/16-\sigma_{001;001}/16-\sigma_{010;010}/8+\sigma_{011;011}/8+\sigma_{1-10;-110}/32-\sigma_{1-11;-111}/32-\sigma_{100;010}/8+\sigma_{101;011}/8+\sigma_{110;110}/32-\sigma_{111;111}/64, \tag{B14}$$

$$f_c=7\sigma_{-1-10;-101}/16+\sigma_{-100;-111}/16+\sigma_{-100;001}/8+\sigma_{0-10;-111}/16-\sigma_{000;001}/8-7\sigma_{010;111}/16-\sigma_{1-10;011}/8, \tag{B15}$$

$$j_c=\sigma_{-1-10;-101}/32-\sigma_{-100;-111}/32-\sigma_{-100;001}/16-\sigma_{0-10;-111}/32+\sigma_{000;011}/16-\sigma_{010;111}/32+\sigma_{1-10;011}/16, \tag{B16}$$

$$f_l=-\sigma_{-1-10;-101}/4+\sigma_{-100;-111}/4-\sigma_{-100;001}/2+\sigma_{0-10;-111}/4+\sigma_{000;011}/2+\sigma_{0101;11}/4-\sigma_{1-10;011}/2, \tag{B17}$$

$$j_l=\sigma_{-1-10;-101}/8-\sigma_{-100;-111}/8-\sigma_{-100;001}/4-\sigma_{0-10;-111}/8+\sigma_{000;011}/4-\sigma_{010;111}/8+\sigma_{1-10;011}/4, \tag{B18}$$

$$y_l(\sigma_{-1-11;-1-11}+2\sigma_{-111;-111}+2\sigma_{1-11;-111}+\sigma_{111;111})/4=\sigma_{-1-11;-1-11}+2\sigma_{-111;-111}+\sigma_{111;111}/4, \tag{B19}$$

$$y_c(\sigma_{-1-11;-1-11}+4\sigma_{-101;-101}+2\sigma_{-111;-111}+8\sigma_{-111;001}+4\sigma_{0-11;-101}+4\sigma_{001;001}+4\sigma_{011;011}+2\sigma_{1-11;-111}+4\sigma_{101;011}+\sigma_{111;111})/16=\sigma_{-1-11;-1-11}+4\sigma_{-101;-101}+2\sigma_{-111;-111}+4\sigma_{001;001}+4\sigma_{011;011}+\sigma_{111;111}/16, \tag{B20}$$

$$z_c(\sigma_{-110;-110}/8+\sigma_{000;-110}/2+\sigma_{000;000}/4+\sigma_{010;010}/2+\sigma_{1-10;-110}/8+\sigma_{100;010}/2+\sigma_{110;110}/8)=\sigma_{-110;-110}/8+\sigma_{000;000}/4+\sigma_{010;010}/2+\sigma_{110;110}/8. \tag{B21}$$

[1] I. V. Hertel, H. Schmidt, A. Bahring, and E. Meyers, Rep. Prog. Phys. **48**, 375 (1985).

[2] E. E. B. Campell and I. V. Hertel, Adv. Chem. Phys. **72**, 37 (1988).

[3] S. R. Leone, Acc. Chem. Res. **25**, 71 (1992).

[4] L. Kovalenko, in *The Chemical Dynamics and Kinetics of Small Radicals*, edited by K. Liu and A. Wagner (World Scientific, Singapore, 1995), p. 730.

[5] M. P. I. Manders, J. P. J. Driessen, H. C. W. Beijerinck, and B. J. Verhaar, Phys. Rev. A **37**, 3237 (1988).

[6] E. M. Spain, M. J. Dalberth, P. D. Kleiber, and S. R. Leone, J. Chem. Phys. **102**, 9532 (1995).

[7] W. Bussert, D. Neuschafer, and S. R. Leone, J. Chem. Phys. **87**, 3833 (1987).

[8] H. A. J. Meijer, T. J. C. Pelgrim, H. G. M. Heideman, R. Morgenstern, and N. Andersen, J. Chem. Phys. **90**, 738 (1989).

[9] J. G. Kircz, R. Morgenstern, and G. Nienhuis, Phys. Rev. Lett. **48**, 610 (1982).

[10] M.-X. Wang, J. Keller, J. Boulmer, and J. Weiner, Phys. Rev. A **35**, 934 (1987).

[11] H. V. Parks, E. M. Spain, J. E. Smedley, and S. R. Leone, Phys. Rev. A **58**, 2136 (1998).

[12] T. L. D. Collins, A. J. McCaffery, and J. N. Wynn, Phys. Rev. Lett. **66**, 137 (1991).

[13] S. S. Op de Beek, J. P. J. Driessen, K. H. J. M. Robben, H. C. W. Beijerinck, and B. J. Verhaar, Phys. Rev. A **56**, 2833 (1997).

[14] J. M. Mestdagh, J. P. Visticot, P. Meynadier, O. Sublemontier,

and A. G. Suits, J. Chem. Soc., Faraday Trans. **89**, 1413 (1993).
[15] J. P. J. Driessen and L. Eno, J. Chem. Phys. **97**, 5532 (1992).
[16] J. P. J. Driessen and S. R. Leone, J. Phys. Chem. **96**, 6136 (1992).
[17] M. H. Alexander, P. J. Dagdigian, and A. E. DePristo, J. Chem. Phys. **66**, 59 (1977).
[18] J. Reuss and S. Stolte, Physica (Amsterdam) **42**, 111 (1969).
[19] J. L. Kinsey, J. W. Riehl, and J. S. Waugh, J. Chem. Phys. **49**, 5269 (1968).
[20] A. M. Arthurs and A. Dalgarno, Proc. R. Soc. London, Ser. A **256**, 540 (1960).
[21] G. Nienhuis, Phys. Rev. A **26**, 3137 (1982).
[22] A. P. Hickman, J. J. Portman, S. Krebs, and W. Meyer, Phys. Rev. Lett. **72**, 1814 (1994).
[23] L. J. Kovalenko, S. R. Leone, and J. B. Delos, J. Chem. Phys. **91**, 6948 (1989).
[24] G. C. Schatz, L. J. Kovalenko, and S. R. Leone, J. Chem. Phys. **91**, 6961 (1989).
[25] B. Huynh, O. Dulieu, and F. Masnou-Seews, Phys. Rev. A **57**, 958 (1998).
[26] D. M. Jones and J. S. Dahler, Phys. Rev. A **35**, 3688 (1986).
[27] I. Y. Yurova, J. Phys. B **28**, 999 (1995).
[28] N. Boutassetta, A. R. Allouche, and M. Auber-Frecon, Phys. Rev. A **53**, 3845 (1996).